Evaluation of an auditory model for echo delay accuracy in wideband biosonar

Mark I. Sanderson[a)]
Department of Neuroscience, Brown University, Providence, Rhode Island 02912

Nicola Neretti
Brain Sciences, Brown University, Providence, Rhode Island 02912

Nathan Intrator
Institute for Brain and Neural Systems, Brown University, Providence, Rhode Island 02912

James A. Simmons
Department of Neuroscience, Brown University, Providence, Rhode Island 02912

(Received 27 November 2002; revised 23 May 2003; accepted 16 June 2003)

In a psychophysical task with echoes that jitter in delay, big brown bats can detect changes as small as 10–20 ns at an echo signal-to-noise ratio of ~49 dB and 40 ns at ~36 dB. This performance is possible to achieve with ideal coherent processing of the wideband echoes, but it is widely assumed that the bat's peripheral auditory system is incapable of encoding signal waveforms to represent delay with the requisite precision or phase at ultrasonic frequencies. This assumption was examined by modeling inner-ear transduction with a bank of parallel bandpass filters followed by low-pass smoothing. Several versions of the filterbank model were tested to learn how the smoothing filters, which are the most critical parameter for controlling the coherence of the representation, affect replication of the bat's performance. When tested at a signal-to-noise ratio of 36 dB, the model achieved a delay acuity of 83 ns using a second-order smoothing filter with a cutoff frequency of 8 kHz. The same model achieved a delay acuity of 17 ns when tested with a signal-to-noise ratio of 50 dB. Jitter detection thresholds were an order of magnitude worse than the bat for fifth-order smoothing or for lower cutoff frequencies. Most surprising is that effectively coherent reception is possible with filter cutoff frequencies well below any of the ultrasonic frequencies contained in the bat's sonar sounds. The results suggest that only a modest rise in the frequency response of smoothing in the bat's inner ear can confer full phase sensitivity on subsequent processing and account for the bat's fine acuity or delay.
[DOI: 10.1121/1.1598195]

PACS numbers: 43.80.Lb, 43.64.Bt [WA]

I. INTRODUCTION

It is widely accepted from behavioral and physiological evidence that echolocating bats determine the distance to objects, or target range, from the time delay of frequency-modulated (FM) echoes (Grinnell, 1995; O'Neill, 1995; Schnitzler and Henson, 1980; Simmons, 1973, 1980, Simmons and Grinnell, 1988; Sullivan, 1982). In two-choice or yes–no discrimination tests, big brown bats (*Eptesicus fuscus*) can distinguish differences in echo delay as small as 50–100 μs (equivalent to 1–2 cm of target range; Moss and Schnitzler, 1995; Simmons and Grinnell, 1988). These behavioral thresholds are roughly consistent with the lower limits (~100–300 μs) for the accuracy of echo-delay registration by response latency in single neurons of the big brown bat's auditory midbrain, and the sharpness of delay tuning in individual forebrain neurons (Dear *et al.*, 1993; Feng *et al.*, 1978; O'Neill and Suga, 1982; Pollak *et al.*, 1977). However, big brown bats can detect much smaller changes in delay in a different behavioral procedure where echoes jitter in delay from one broadcast to the next (Moss and Schnitzler, 1995). In several versions of the jittering-echo experiment, conducted in two different laboratories, bats were able to detect changes as small as 0.5–1 μs (Menne *et al.*, 1989; Moss and Schnitzler, 1989; Moss and Simmons, 1993). The bat's threshold for jitter was measured to be 10–15 ns when an apparatus was developed to test even smaller delay jitter (Simmons *et al.*, 1990). At a controlled echo signal-to-noise ratio of 36 dB, big brown bats can detect delay changes as small as 40 ns, which actually is possible from an information-theoretic perspective if the bats used several successive broadcasts to judge whether echoes jittered in delay (Simmons *et al.*, 1990). Nevertheless, the degree of temporal precision required to support this performance has been described as virtually impossible for the auditory system to achieve, so the ''10-ns result'' is widely assumed to be due to an artifact, most likely spectral in nature, rather than perception of such small changes in time (Beedholm and Mohl, 1998; Menne *et al.*, 1989, Pollak, 1993; Schnitzler *et al.*, 1985). The work reported here concerns whether models of peripheral auditory transduction and coding are in fact unable to support submicrosecond delay perception at levels achieved by echolocating bats.

a)Electronic mail: mark_sanderson@brown.edu

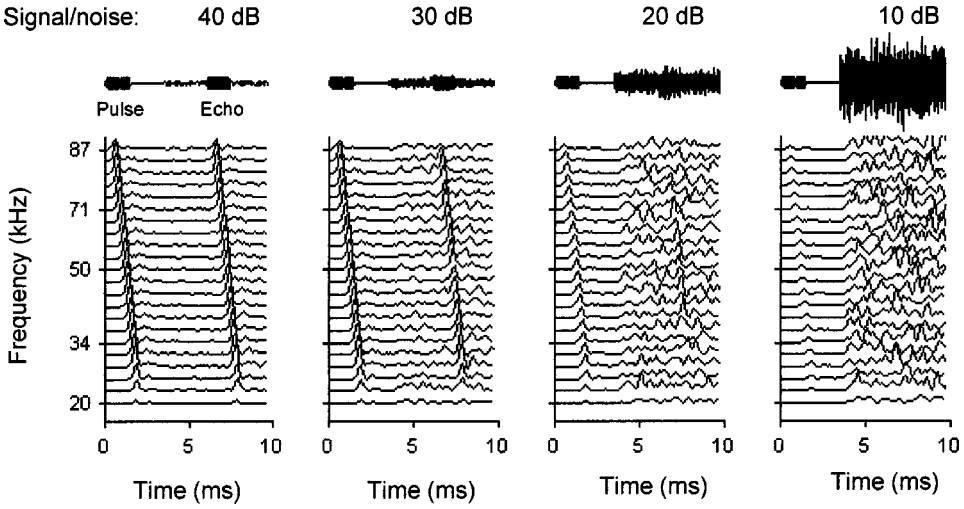

FIG. 1. Time waveforms and their filterbank output for different signal-to-noise ratios. A pulse (90–20 kHz, linear FM) was followed by an echo at 6-ms delay. The pulse and echo are identical, except that bandlimited noise (90–20 kHz) was added to the signal 2 ms after the pulse. The signal-to-noise ratio decreases until the echo is no longer visible, which in these examples occurs at 10 dB. The scale for the time waveforms at top is the same for all signal-to-noise ratios. The filterbank output for each waveform is plotted in the bottom row (see the text for details). The scaling for the four bottom plots varies to display the full data range in each plot.

This paper describes an auditory filterbank model of the bat's auditory periphery and the accuracy of this model for determining echo delay compared to standard sonar signal-processing techniques (cross correlation) as well as a previously used filterbank model of the bat's auditory periphery (Menne and Hackbarth, 1986; Hackbarth, 1986). We simulated the essential signal-processing steps performed by the bat's inner ear in multiple-trial tests to evaluate model performance for detecting jitter in echo delay. These tests allowed us to identify the values of model parameters required to account for the bat's submicrosecond acuity and the 10-ns result. One goal is to guide future physiological experiments by determining whether the bat's performance really is impossible, or whether there is a range of physiologically testable model parameters that makes this performance possible.

The question of the bat's delay acuity has been addressed previously for cross-correlation receivers (Menne and Hackbarth, 1986) and for a simple filterbank receivers (Hackbarth, 1986; Menne, 1988). Although fine delay acuity is possible with cross correlation, it cannot be achieved with the filterbank model as it was constituted originally. We chose to reexamine this question because several aspects of the Hackbarth (1986) filterbank model were unrealistic in auditory terms and several critical parameters have never been measured in bats. In particular, the design of the filterbank's smoothing (low-pass) filters removed all phase information from the envelopes to be processed for echo delay. Because several behavioral experiments have shown that bats may be able to detect changes in relative phase (Altes, 1984; Simmons *et al.*, 1990, Moss and Simmons, 1993), we decided to revisit the question of echo-delay accuracy and focus our attention on the role of the smoothing filter, which had been singled out as a critical stage for replicating the bat's performance (Simmons, 1980). A companion paper (Neretti *et al.*, 2003) addresses the related question of the delay resolution achievable by a similar auditory model. It should be clearly stated that *resolution* and *accuracy* refer to *separate* features of an echo-delay estimator, and the terms should not be used interchangeably (see Schnitzler and Henson, 1980). The accuracy of a delay estimator is the uncertainty in its estimate for the arrival time of echoes from a single reflecting point. In contrast, delay resolution refers to the minimum separation between two nearly simultaneous, overlapping echoes where the two reflections are assigned their own delay estimates instead of being interpreted as a single echo.

II. METHODS

A. Biosonar signals

The characteristics of the model are shown in the left panel of Fig. 1. The procedure for testing the model simulated the bat's biosonar emission, or pulse, in an acoustic environment that contained a single point-like reflector at a target range of ~1 m. For simplicity, the bat's pulse was modeled with a single harmonic, linear frequency-modulated (FM) chirp that swept from 90 to 20 kHz in a total duration of 1.5 ms. The test echo was a copy of the pulse shifted in time by an appropriate delay for a reflector at a range of 1.032 m (6 ms). The pulse and test echo were placed together in a single time record 12 ms long (top traces in Fig. 1).

This simulation assumed, as have other models, that the bat acquires a noise-free estimate, or template, of its outgoing pulse (see Menne and Hackbarth, 1986, Matsuo *et al.*, 2001, Saillant *et al.*, 1993). Bandlimited Gaussian noise (90–20 kHz) was added to the time record beginning 2 ms after the offset of the pulse and continued over the entire epoch in which the echo was embedded (Fig. 1, the 30-dB panel, shows an example of the onset of this noise). The echo signal-to-noise ratio was determined according to the following equation (Menne and Hackbarth, 1986):

$$\text{Signal-to-noise ratio(dB)} = 20\log_{10}(\sqrt{d}), \tag{1}$$

$$d = 2E/N_0, \tag{2}$$

where E is the echo energy flux, or the integral of squared amplitude over the duration of the signal, units are in pascals^{2}s; N_0 is the noise power per unit Hz, or mean-square amplitude divided by bandwidth, units are in pascals^{2}s.

Foraging bats in their natural habitats deal with acoustic environments that consist of more than just a single reflector and Gaussian noise. Instead, bats encounter non-Gaussian atmospheric effects and considerable clutter—other bats' emissions, multiple insects, background vegetation, etc. To

be clear, the noise added in these simulations was *not* meant to simulate noise in the bats' real-world acoustic environment. The added noise simulated only the controlled white noise the bats encountered in psychophysical experiments with jittering echoes (for details on the experimental signal-to-noise ratio, see Simmons *et al.*, 1990). Bats flying in their natural environments often deal with signal-to-noise ratios lower than the 30–50 dB. Nevertheless, our intention was to understand how a signal-processing model performed in a situation similar to that seen by the bat in experiments from which researchers have obtained precise, informative measures of their sonar capabilities.

The echo was just a single delayed reflected replica of the broadcast; Doppler shifts and those scattering properties of the target that affect the echo spectrum were not considered here (See Neretti *et al.*, 2003, for the resolution of a model that deals with multiple echoes.)

The pulse–echo time waveforms for four signal-to-noise ratios are shown in Fig. 1 (top row). For simplicity, the pulse and echo were set to have equal energy, while noise power increases from the left to the right in successive plots. Below the time traces in Fig. 1 are the 22 parallel filterbank outputs, which consist of envelopes that trace the FM sweep in the pulse and the echo in a spectrogram-like format. The location of the echo is obvious in the time waveform and filterbank output for high signal-to-noise ratios (e.g., signal-to-noise ratios 40, 30 dB in Fig. 1). At lower signal-to-noise ratios, however (e.g., 10 dB), the noise swamps the presence of the echo in both the waveform and filterbank displays. Our simulations of echo-delay determination assessed how different versions of the filterbank channels performed in varying levels of noise. Note that this model does not consider the effect that the receiver's internal noise has upon delay accuracy. That is, the filterbank itself and subsequent processing steps are assumed to be noise-free; only the external signal-to-noise ratio is included here.

B. Filterbank

We modeled the bat's cochlea with a filterbank composed of 22 channels, each of which had three components connected in series: a bandpass filter, a half-wave rectifier, and a low-pass filter. The frequency tuning of the ''cochlea'' was implemented with a series of overlapping bandpass filters (Chebyshev IIR filters, constant 4-kHz bandwidth). We chose the Chebyshev design because it allows a narrower bandwidth than the Butterworth design of the same order. Simulation of the transduction and capacitance of the inner hair cell was implemented with a half-wave rectifier and low-pass filter (Chebyshev IIR filters). The resulting output from the low-pass filter corresponded to the probability of neurotransmitter release at the base of the inner hair cell and represented the excitation function delivered to auditory-nerve fibers for coding as spikes. The model's filterbank parameters are listed in Table I. The center frequencies (CFs) for the bandpass filters were chosen to (1) cover the 20–90-kHz frequency range of the big brown bat's hearing (Koay *et al.*, 1997), and (2) to overlap as closely as possible with their neighbors at their 3-dB down points.

TABLE I. Values for various parameters of the filterbank model and delay estimation methods.

Sample rate	2 MHz
Signal	
Duration	1.5 ms
Sweep type	Linear
Harmonics	1
Frequency start	90 kHz
Frequency end	20 kHz
Rise/fall time	0.15 ms, cosine^2 ramp
Bandpass filter	
Number of filters	22; see Table II
Design	Chebyshev type 1 (IIR)
Ripple in passband	6 dB
Order	8
$\text{Bandwidth}_{3\text{dB}}$	4 kHz
Nonlinearity	
Half-wave rect. $y=x$ for $x\geqslant 0$	
$y=0$ for $x<0$	
Low-pass filter	
Design	Chebyshev type 1 (IIR)
Order	2, 5
$\text{Corner}_{3\text{dB}}$ freq.	1, 2, 4, 8, 125 kHz
Other	
A priori window	± 1000 μs

Filter center frequencies were restricted to integer multiples of the 0.5-μs sample period (listed in Table II). This step was to minimize interference between the simulation's sample rate (2 MHz) and filter CF. This restriction provided better digital approximations of the equivalent analog filter impulse responses. Otherwise, if this step was not taken, the outputs of filters with certain CFs exhibited interference effects with the sample rate in the peak region of the impulse

TABLE II. Period and center frequency of the 22 bandpass filters used in the filterbank.

	μs	kHz
1	50	20.000 000 0
2	44	22.727 273 0
3	39.5	25.316 456 0
4	35.5	28.169 014 0
5	32.5	30.769 231 0
6	29.5	33.898 305 0
7	27	37.037 037 0
8	25	40.000 000 0
9	23	43.478 261 0
10	21.5	46.511 628 0
11	20	50.000 000 0
12	19	52.631 579 0
13	18	55.555 556 0
14	17	58.823 529 0
15	16	62.500 000 0
16	15	66.666 667 0
17	14	71.428 571 0
18	13.5	74.074 074 0
19	13	76.923 077 0
20	12.5	80.000 000 0
21	12	83.333 333 0
22	11.5	86.956 522 0

response envelope. If these filters were used to estimate delay the resulting estimates would be biased away from the true peak in the impulse response. Restricting the filter CFs to those in Table II ensured that the digitally implemented impulse responses for all filters had the same envelopes. This minimized any potential bias in the delay estimates in individual channels.

The primary question was how the filterbank receiver's delay accuracy compares against a cross-correlation receiver. Here, we adopted a similar trial-by-trial approach to that used previously (Menne and Hackbarth, 1986; Hackbarth, 1986). The task was to estimate the delay between a pulse and a single echo at a fixed delay for multiple occurrences of the pulse and the echo. We implemented four delay estimation methods for comparison purposes.

C. Delay estimation methods

Three methods (''analog sum,'' ''Saillant,'' and ''Hackbarth'' methods) were used to estimate the delay between events corresponding to the pulse and echo generated by the filterbank. Our interest was focused on how the filterbank design parameters, not the different delay estimation methods, affected delay estimation accuracy. The estimation methods described below were not intended to realistically model the full range of physiological processes that the bat auditory system uses to estimate pulse–echo delay subsequent to auditory transduction by the inner ear. Instead, the aim was to measure, with the best precision possible, the temporal intervals between events in the filterbank channels.

1. Cross correlation

To obtain an optimal (matched-filter) delay estimate, we first computed the cross-correlation function between the noise-free pulse and the echo embedded in noise for each noise iteration at each signal-to-noise ratio. Then, the peak in the cross-correlation function was located within an *a priori* window ± 1000-μs window around the true delay (as in Menne and Hackbarth, 1986 and Hackbarth, 1986). Finally, the three points around the peak were fit with a quadratic function in order to determine the peak's precise position. By this interpolation procedure, delay estimates could be ''recorded'' with a precision greater than the 0.5-μs sample period we used to generate our pulse and echo signals.

The time-estimation process was repeated for each of the 400 trials with independent noise samples in a Monte Carlo procedure (see below). The delay estimate for each trial can be compared against the theoretical accuracy possible for a cross-correlation receiver (Burdic, 1968)

$$\sigma = (2\pi B d)^{-1}, \tag{3}$$

where d is from Eq. (2), and B is the sonar emission's noncentralized root-mean-square bandwidth, which for this simulation equaled 57.79 kHz. This value was slightly higher than the typical value, ~55 kHz, estimated for signals recorded in psychophysical experiments (Simmons *et al.*, 1990). The cross-correlation approach did not use the output from the filterbank, whereas the next three methods did.

2. Analog sum method

The second method for estimating delay, which will be called the ''analog sum'' approach, used the ''cochlear'' filterbank to process broadcasts and echoes. First, the output of all the filter channels was dechirped to remove the slope of the FM sweep by aligning the peaks of the outputs for the emitted pulses. Peaks for the broadcast in individual channels were located by finding the highest value in the channel output over the time window containing the broadcast [see Fig. 2(C)] and sliding each time series signal by a corresponding amount to align the peaks in different channels to the same reference time value. Then, the dechirped output was summed across all frequency channels [Fig. 2(B)], and the position of the peak in the resulting sum was located within an *a priori* window ± 1000 μs around the true delay. Finally, using a quadratic fit, the interpolated peak location was determined and stored as the overall estimate for echo delay. Thus, as for cross correlation, delay estimates have a higher precision than the 0.5-μs sampling interval. This process was repeated for each of the 400 trials with independent noise samples in a Monte Carlo procedure (see below).

3. Hackbarth method: Single peak detection followed by interval measurement

This approach, described by Hackbarth (1986), also used the filterbank to process broadcasts and echoes. First, the location of the peak in the output from each filter channel for the noise-free pulse was located inside a window from time zero to 3.5 ms (Fig. 1). Then, the peak for the echo was located inside the *a priori* window of ± 1000 μs centered on 6 ms after the peak for the broadcast [Fig. 2(C)]. Following this initial procedure, the method produced single triggered events for the pulse and for the echo. The method

(a) fit the three points around the pulse and echo peak samples with quadratic functions in order to determine their exact positions, which were marked by single pulses [this was performed separately for the pulse and echo response in each frequency channel, Figs. 2(D) and (E)];
(b) measured first-order intervals by subtracting the time of the interpolated pulse peak from the interpolated echo peak in each frequency channel [Fig. 2(F)];
(c) generated a point process by projecting these intervals across filterbank channels onto a single time axis [Fig. 2(G)];
(d) estimated the density of the point process along the time axis by convolving the points with a Gaussian kernel ($\sigma = 1$ μs, shift step $= 0.25$ μs [Fig. 2(H)]; and
(e) located the peak of the density function resulting from convolution by fitting a quadratic to the peak sample and its two neighboring samples, as before, and stored this interpolated value as the *overall delay estimate* for that trial.

This process was repeated for each of the 400 trials with independent noise samples in a Monte Carlo procedure (see below).

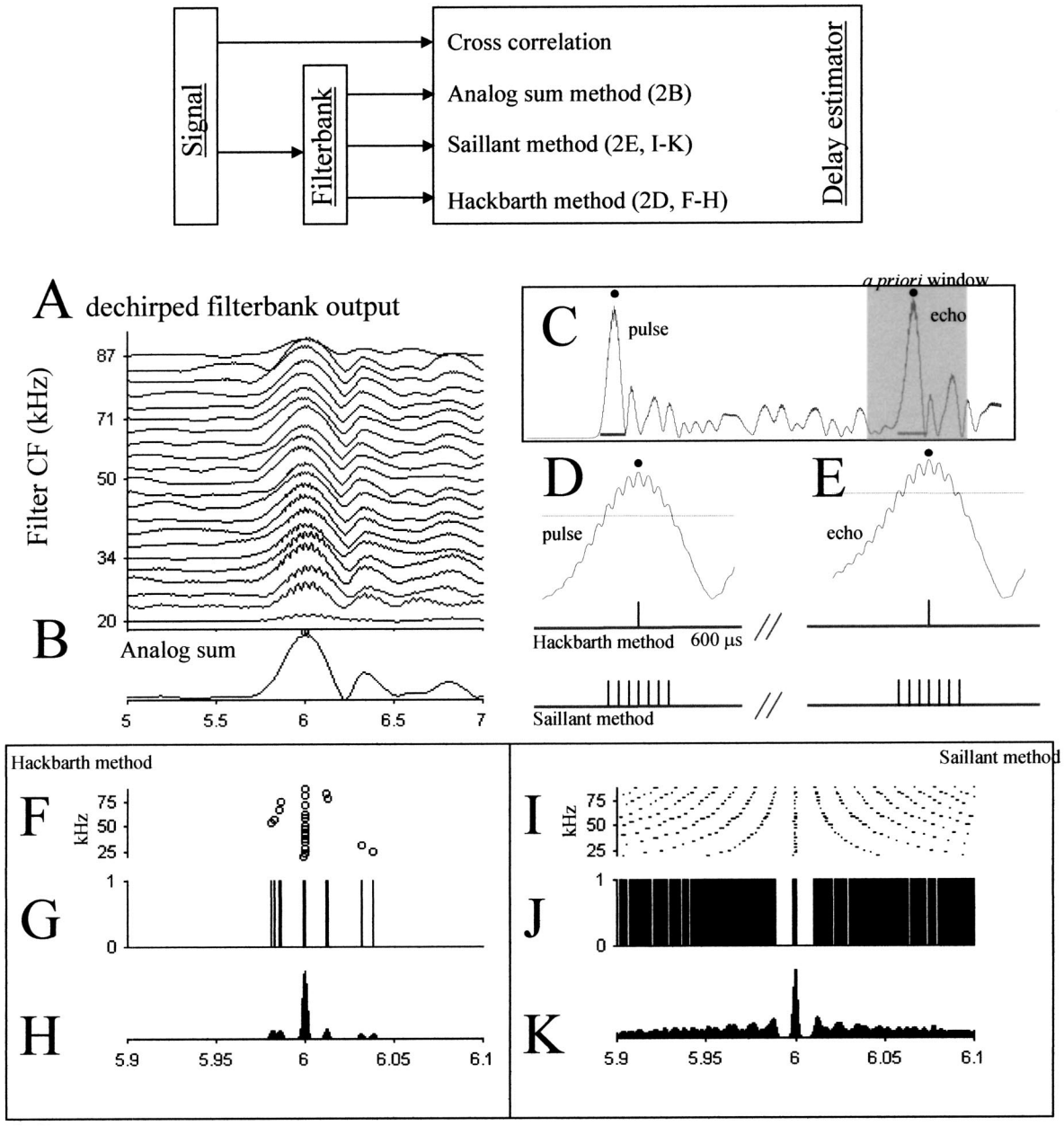

FIG. 2. Three methods for estimating delay from the filterbank output. The schematic at top illustrates how the biosonar signal passes through the filterbank, the output of which is processed by three different estimators. The cross-correlation estimator operates directly on the pulse–echo signals. (A) Dechirped output from a filterbank with a second-order low-pass filter cutoff set to 8 kHz, and a signal-to-noise ratio of 36 dB. (B) The summed output, across frequency channels, from panel (A). The peak position is the ''analog sum'' method's echo delay estimate. (C) Output from the filterbank's third channel (CF $=25.3$ kHz). (D) Expanded view of the pulse [corresponds to left gray bar in panel (C)]. Spikes are triggered by the maximum peak for the Hackbarth method and for the local peaks above a threshold for the Saillant method. (E) Expanded view of the echo with triggered spikes for both methods at bottom. (F) Interpolated delay estimates from the Hackbarth method. (G) Histogram of peaks from (F). (H) Smoothed histogram from (G), using Gaussian kernel with $\sigma=1$ μs. The interpolated peak is the Hackbarth method's final delay estimate. (I–K) Same as (F)–(H) but for the Saillant method. Note that x axes for (F)–(K) range from ±100 μs, whereas (A) and (B) range from ±1000 μs relative to actual echo delay.

4. Saillant method: Detection of multiple peaks followed by all-order interval measurement

This final method created a series of triggered spike events for the pulse and then for the echo using a procedure similar to the ''peak-detection'' approach of Saillant *et al.* (1993). First, the peak position in the noise-free window for the pulse in each filterbank channel was located (as above), and the corresponding sample times across channels were used to dechirp the filterbank output (each channel's time axis was realigned so the peak pulse time corresponded to time zero). Then, the model generated spikes within two *a priori* windows: one centered on the pulse and one on the echo. The pulse *a priori* window spanned the noise-free time window from time zero to 3.5 ms (Fig. 1). As before, the echo *a priori* window spanned ±1000 μs and was centered in time at the true echo delay.

For each filterbank channel, separate thresholds were set for the pulse and echo to define the time windows inside

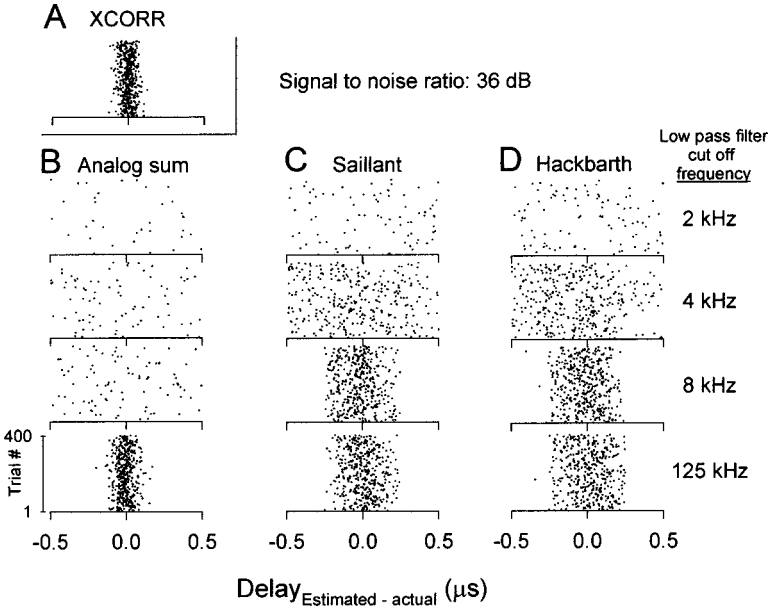

FIG. 3. Results from 400 Monte Carlo trials with echo signal-to-noise ratio fixed at 36 dB. (A) The cross-correlation receiver's estimates. (B), (C), and (D) Results for each of the three filterbank models are plotted in separate columns. As the low-pass filter cutoff frequency increased, the variability of the delay estimates decreased (1-kHz results not shown). Because the *x* axis is scaled so that only the central 1 μs of the full $\pm$ 1000-μs *a priori* window is visible, some of the estimates are not visible (especially for the 1- and 2-kHz low-pass filter conditions). The accuracy of each method was estimated by taking $\frac{1}{2}$ of the 68th percentile of the distribution of delay estimates, and is summarized in Fig. 4.

which multiple peaks in the filter output would registered as corresponding multiple spikes. For the pulse, the spike-window threshold was set at the value of 67% of the peak amplitude within the previously defined pulse *a priori* window. For the echo, the first step was to establish a noise threshold located 2 standard deviations above the mean noise level in the filter output over a time window containing just noise. In the second step, the echo spike-window threshold was set at the value 2/3 of the way between this noise threshold and the amplitude of the largest peak within the echo *a priori* window. Spike events then were generated for every local peak above the pulse-window and echo-window thresholds [see Figs. 2(D) and (E), respectively], and the location of each local peak was identified using interpolation (as before, a quadratic was fit to each local peak and the immediate neighboring samples). At this juncture, the channel-by-channel filterbank output is converted into two sets of spike events corresponding to all the local peaks within the pulse and echo windows [one channel's output shown in bottom panel of Figs. 2(D) and (E)].

To obtain a single estimate for pulse–echo delay from this multiple-spike representation, the method

(a) calculated the all-order intervals (Cariani and Delgutte, 1996) for pulse versus echo spikes within each channel [Fig. 2(I)];
(b) generated a point process by projecting these resulting intervals onto a single time axis [Fig. 2(J)];
(c) estimated the density of the point process along the time axis by convolution with a Gaussian kernel [$\sigma = 1$ μs, shift step$=0.25$ μs; Fig. 2(K)]; and
(d) located the peak of the resulting density function by fitting a quadratic to the peak sample and its two neighboring samples and stored it as the *overall delay estimate* for that trial.

This process was repeated for each of the 400 trials with independent noise samples in a Monte Carlo procedure (see below).

D. Monte Carlo trials

Our goal was to examine how the use of different filterbank parameters affected the variance of the delay estimation procedure. To estimate this variance we adopted a Monte Carlo procedure, a method that uses many independent trials, each with a different noise instantiation, in order to build a distribution of the delay estimates. The variance of the delay estimation procedure is then measured from this distribution. The number of trials used in the Monte Carlo simulations do not improve the accuracy of the model because there is no memory from trial to trial in the Monte Carlo method. Our results were identical using 100 or 400 trials. It follows that the number of Monte Carlo trials bear no relation to how many emissions the bats actually use in a single trial of the jitter task.

Pulse–echo delay estimation was repeated for 400 different realizations of noise added to the echo at a fixed signal-to-noise ratio [Fig. 3]. The true echo delay, 6 ms, was subtracted from each of the 400 estimates to form the error distribution. To estimate the mean and variance of the accuracy of this distribution we used a bootstrap procedure. Four hundred samples were drawn, with replacement, from the error distribution, and the 68th percentile was calculated. The resulting value was divided by 2 in order to match the standard deviation for a uniform distribution in a 1000-ms window ($\sim$683 μs). This sampling was then repeated 128 times to compute the bootstrapped estimate for the mean and standard deviation of accuracy.

The bootstrapped accuracy estimates are plotted in Fig. 4 against the range of signal-to-noise ratios tested. This method for estimating the estimates' variability was used for comparison with other models (Hackbarth, 1986, Menne and Hackbarth, 1986) and the analytical standard deviation calculation [see Eq. (3) above].

E. Additional constraints

The width (σ) of the Gaussian kernel chosen for the smoothing procedure affected the estimate of filterbank ac-

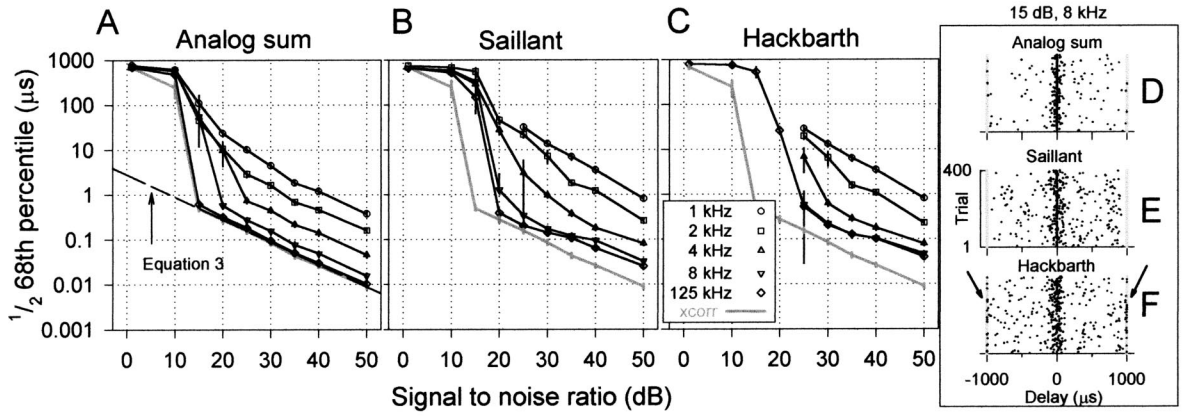

FIG. 4. Filterbank accuracy with different low-pass filter settings. The accuracy of the cross-correlation Monte Carlo simulations is plotted as a heavy gray line on each panel for comparison. (A) The accuracy of the analog sum method when applied to the filterbank output. Five different settings for the filterbank's low-pass filter were used [see the legend in panel (C)]. Increasing the low-pass filter cutoff value shifted the analog sum method's accuracy much closer to that of the cross correlation. The values for Eq. (3) are plotted as a dashed line. (B) Same as (A) except delay estimates were generated by applying the Saillant method to filterbank output. (C) Same as (A) except delay estimates were generated applying the Hackbarth method to filterbank output. (D)–(F) These three plots show the 400 trial-by-trial estimates for the analog sum, Saillant, and Hackbarth methods. Note that for the Hackbarth method, many estimates occur at the edges of the *a priori* window.

curacy (step *e* of the Hackbarth method and step *d* of the Saillant method). If the Gaussian was too wide relative to the ''true'' accuracy of the filterbank, all of the trial-by-trial estimates fell within a single bin. This underestimated the effective accuracy of the filterbank. On the other hand, if the Gaussian width was too narrow, the smoothing step resulted in multiple local peaks with equal heights and so failed to yield a single delay estimate. After testing of sample data with several different values for σ of the Gaussian kernel, we chose the value that yielded the maximum accuracy ($\sigma = 1$ microsecond).

The size of the *a priori* window also has a significant effect on the accuracy of each receiver design, as shown previously in Menne and Hackbarth (1986) and Hackbarth (1986). However, the *a priori* window size only affects the accuracy of the results within a fixed range of signal-to-noise values less than 15 dB, where the accuracy curve ''breaks'' or undergoes an abrupt decline due to ambiguity effects caused by the emergence of prominent sidelobes (Menne and Hackbarth, 1986). We chose the value of +/−1000 microseconds for our *a priori* window in order to compare our results with theirs. The use of *a priori* windows with respect to biosonar experiments is not unreasonable: the bat certainly knows when it vocalized its pulse, and in behavioral paradigms learns fairly quickly that most echoes return within a fixed time window.

F. Simulation of the jittering-echo experiment

In the jittering-echo experiment, the bat is trained to sit on a small platform and emit sonar sounds into microphones, and its task is to determine which of two loudspeakers returned echoes of those sounds that alternated in delay from one broadcast to the next (Simmons *et al.*, 1990). In individual jitter trials, the bat necessarily emitted at least two sounds to the jittering stimulus channel and two sounds to the nonjittering channel. A single stimulus echo was returned for each emission, the delay of which was fixed on one side and jittered between two values on the other side. The bat estimated each returning echo's delay for comparison with the delay of the next echo to then choose which side had the jittering echoes.

We simulated this experiment, following the method of Menne and Hackbarth (1986), in which the virtual bat discriminated a jittering target from a nonjittering target. On one ''side'' the virtual bat received two echoes embedded in noise at a fixed delay. On the other ''side'' the virtual bat received two echoes in noise with a temporal offset, or jitter, added to each echo. The data for the experiment had in fact been simulated under different conditions in the Monte Carlo simulations. We could therefore simply draw four delay estimates, without replacement, from these simulations and a temporal offset $(+\Delta t, -\Delta t)$ was added to the two delay estimates on the jittering ''side.'' On a single trial the virtual bat had to decide which side had the jittering echoes. The jitter experiment was simulated with 100 such trials, and the results of the simulation were expressed as the percentage of correct decisions for those 100 trials for different values of Δt (the amount of jitter, Δt, was varied from 0 to 20 microseconds). This entire procedure was then repeated 128 times to compute a bootstrap estimate of the variability for these percent-correct values.

III. RESULTS

A. Monte Carlo results

The results consist of a series of estimates of delay accuracy obtained with each of the four model designs on 400 Monte Carlo trials at each signal-to-noise ratio. To illustrate the nature of the simulation results, the 400 trial-by-trial delay estimates obtained with the four methods are plotted for one signal-to-noise ratio (36 dB) and different low-pass smoothing frequencies (1, 2, 4, 8, and 125 kHz) in Fig. 3. To establish a baseline for comparison, the performance of the cross-correlation procedure is show in Fig. 3(A), while the results from the three filterbank methods are plotted in sepa-

rate columns [Figs. 3(B)–(D)]. Each point on one of the graphs represents a single delay estimate for a pulse–echo pair with one iteration of independent noise added to the echo. All four methods generated well-behaved delay estimates across the Monte Carlo trials, and in each case the variability of the estimates changed with the low-pass cutoff. With increasing low-pass cutoff frequency, the variability of each distribution decreases appreciably (except for the Hackbarth method, for which the results at 8 and 125 kHz were very similar—that is, once the low-pass cuttoff was as high as 8 kHz, no further improvement in accuracy could be obtained). The 125-kHz low-pass filter condition was explicitly included in the simulations to observe what happened when all the available phase information was allowed to pass through the model and made available for processing (this was our method for the effective removal of the low-pass filter). As such, the analog sum method with a 125-kHz low-pass filter yielded the tightest distribution of delay estimates, a distribution that was indistinguishable from the results for the optimal delay estimator, the cross-correlation receiver, plotted in Fig. 3(A).

The summary and quantification of the variability of all delay estimates across a wide range of signal-to-noise ratios is plotted in Fig. 4. These curves show the effects of the low-pass filter parameters on the accuracy of delay estimates, and allow comparison of the performance for different estimation methods.

1. Cross-correlation accuracy

Because the cross-correlation receiver's accuracy was the lower bound to be expected for the various estimation methods, it is shown on each plot in Fig. 4 as a baseline. The cross-correlation results from the Monte Carlo trials fit the theoretical accuracy [Eq. (3), dashed line] for high signal-to-noise ratios ($>$15 dB). Between signal-to-noise ratios of 15 to 10 dB, the cross-correlation receiver accuracy falls off sharply compared to what theory predicts. The nature of this break in the cross-correlation performance was explored previously by Menne and Hackbarth (1986). They showed that Eq. (3) was applicable only when the signal noise ratio was above 15 dB, and our results are the same.

2. Filterbank model accuracy: Analog sum method

The analog sum method yielded results almost identical to the cross correlation when the entire signal bandwidth passed the low-pass filter (i.e., cutoff frequency$=$125 kHz). This shows that bandpass filtering, rectification, and peak picking had no deleterious effects on accuracy. However, as high-frequency phase information was progressively removed from the filterbank output by the low-pass filter, accuracy degraded precipitously. In the linear region of the results (signal-to-noise ratio $\geqslant$30 dB), the accuracy of delay estimation degraded by 2 orders of magnitude as the low-pass cutoff frequency was decreased from 125 to 1 kHz. Between signal-to-noise ratios of 20 and 15 dB, the accuracy curves break sharply from the linear case and eventually converge upon the standard deviation for the whole *a priori* window, 680 μs.

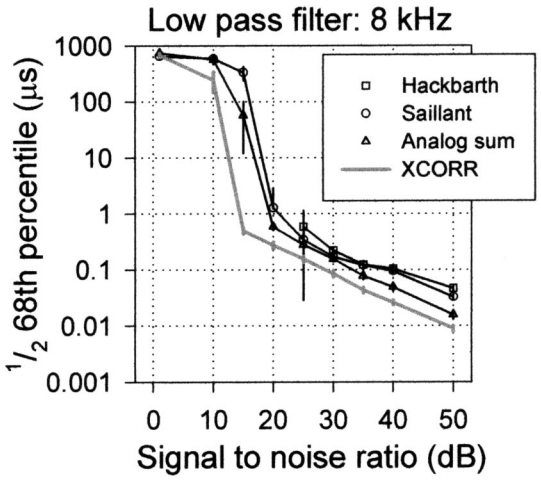

FIG. 5. Comparison of different filterbank delay estimation methods when using a second-order low-pass filter set at 8 kHz. Of the filterbank estimators, the analog sum method provided the best performance. There was an orderly arrangement to where each method ''broke,'' or underwent a sharp transition in accuracy: the cross-correlation accuracy broke between 15 to 10 dB, the analog sum method between 20 and 15 dB, the Saillant method between 25 and 20 dB, and the Hackbarth method between 30 and 25 dB. The Hackbarth and Saillant methods were identical for signal-to-noise ratios $\geqslant$30 dB.

3. Filterbank model accuracy: Saillant method

The Saillant method used one or more spikes to mark the occurrence of the pulse and echo in each channel [Figs. 2(D) and (E)]. As such, it uses less of the filterbank output's wave structure, compared to the analog sum method, to estimate pulse–echo delay and so would be expected to do worse at any given signal-to-noise ratio. In Fig. 4, the performance of the Saillant method is displaced upward relative to the analog sum method to slightly worse performance across most signal-to-noise ratios. This is more clearly shown in Fig. 5, which plots the performance of all four methods at an 8-kHz low-pass cutoff.

4. Filterbank model accuracy: Hackbarth method

In each frequency channel the Hackbarth method used only one spike to mark the occurrence of the pulse and one spike for the echo (see Fig. 2). At signal-to-noise ratios $\geqslant$30 dB, the accuracy results for the Hackbarth method were very similar to those of the Saillant method. The exception was the 125-kHz low-pass filter condition, which for the Hackbarth method did not show any appreciable difference from its 8-kHz result.

Unlike the Saillant method, we observed that for signal-to-noise ratios below 25 dB the *a priori* window size interacted with the low-frequency nature of the filterbank output. The width or duration of the ''excitation'' in each frequency channel was a function of the signal sweep rate, integration time, and low-pass filter time constant. Because the excitation half-width was about 250–300 μs [Fig. 2(D)], the outputs of the filters were such slowly varying signals that they could almost be considered as linear when viewed within a small *a priori* window. Consequently, the signals often reached their maximum at one of the window edges [Figs. 3(D), (E), (F)]. Because of this edge effect, we discarded any

accuracy measurements if a conspicuous number (>10%) of trials resulted in delay estimates at the edges of the *a priori* window.

Figure 4(F) shows the trial-by-trial results for the Hackbarth method at a low signal-to-noise ratio. Many of the data points for delay estimates fall on top of the gray bands that mark the edges of the *a priori* window. The analog sum and Saillant methods do not suffer from this problem [Figs. 4(D), (E)]. Although this edge effect was not reported in Hackbarth (1986), she also only plotted results for signal-to-noise ratio values above 20 dB, so we assume she had the same problem in her analysis. Because the Saillant method triggered spikes from *multiple* local peaks above threshold [e.g., Fig. 2(E)], it did not suffer from this edge effect when the low-pass cutoff frequency was >2 kHz.

5. Comparison of the three filterbank methods

Figure 5 shows, for a single 8-kHz low-pass filter condition, the performance of the three filterbank methods on the same plot. From Fig. 5 it was clear that (1) the analog sum method provided the best accuracy (other than the cross-correlation method), and (2) the points where the slope of the curve changed sharply for each method were separated along the horizontal signal-to-noise axis by about 5 dB.

6. Steeper roll-off for the low-pass filter

We also investigated how the severity of low-pass filtering affected the accuracy of the three filterbank delay estimation methods. The second-order Chebyshev low-pass filter had a roll-off of 22 dB/decade. This was rather shallow compared to the 100-dB/decade value estimated for the mammalian smoothing filter (Weiss and Rose, 1988). Therefore, we repeated the simulations using a fifth order Chebyshev low-pass filter that provided attenuation of 62 dB/decade. This more severe low-pass filtering removed most of the ripple riding on each frequency channel's envelope. Consequently, the filterbank performance decreased by 25 dB for all three methods (Fig. 6; Hackbarth method not shown). In addition, the loss of any significant ripple meant that the Saillant method no longer could trigger multiple spikes for the pulse or echo. Consequently, the Saillant and Hackbarth methods converged on using the same single local peak for the pulse and for the echo to generate their spike events, and they yielded similar results.

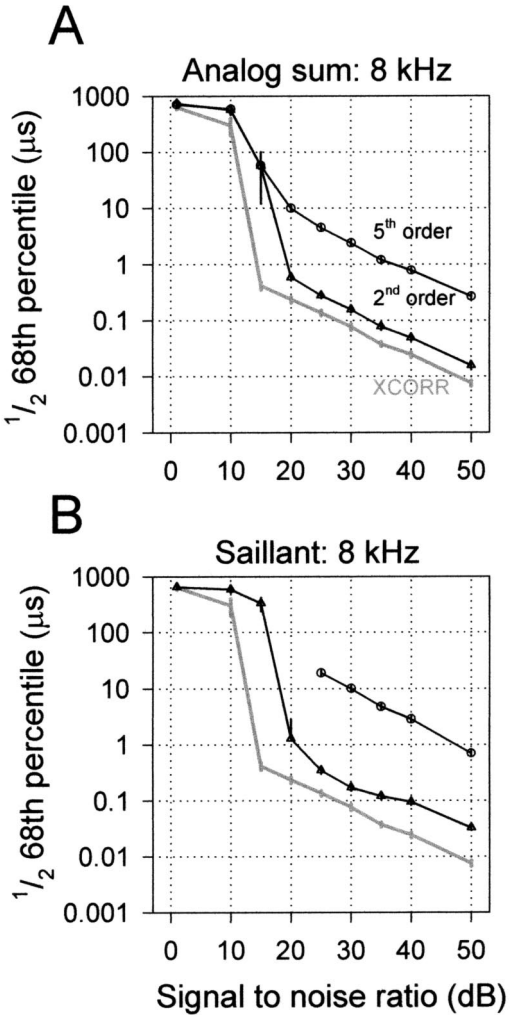

FIG. 6. Increasing the severity of low-pass filtering drastically reduced filterbank accuracy. (A) When the order of the low-pass filter was increased from 2 to 5, the analog sum method's results shifted by about 25 dB. (B) Same as (A), but for the Saillant method.

B. Simulation of the jittering-echo experiment

The performance of the analog sum filterbank model in the jitter experiment is shown in Fig. 7(A). At a signal-to-noise ratio of 36 dB, as in the original behavioral experiment (Simmons *et al.*, 1990), the curves for percent correct show better performance (shift to the left) with increasing cutoff frequency for the low-pass filter. The threshold for jitter detection, Δt_{75}, was taken at the value that resulted in a performance of 75% correct (actual value was identified using cubic spline interpolation).

The thresholds for the cross correlation, analog sum, and Saillant method are shown in Fig. 7(B). The 40-ns threshold, which was measured in the behavioral experiments at a signal-to-noise ratio of 36 dB, is also plotted for comparison. At this signal-to-noise ratio, the best filterbank method (analog sum with a second-order low-pass filter) had a jitter threshold of 82.9 ns. The analog sum method required a rather high SNR, 50 dB, in order to achieve 16.6-ns jitter detection performance based on the two pairs of echoes as simulated stimuli.

IV. CONCLUSIONS

These modeling results show that low-pass filtering strongly affects the accuracy of a filterbank receiver. For bats, this means that achieving 40-ns jitter acuity at a signal-to-noise ratio of ~36 dB requires that cochlear bandpass and low-pass filtering properties adhere to the following two constraints: First, the bandpass filters' integration time should match the sweep rate of the FM emission (discussed previously in Menne, 1988). Second, the effective low-pass filtering that takes place before auditory-nerve spike generation should have, compared to typical mammalian values, a rather high cutoff frequency and shallow slope.

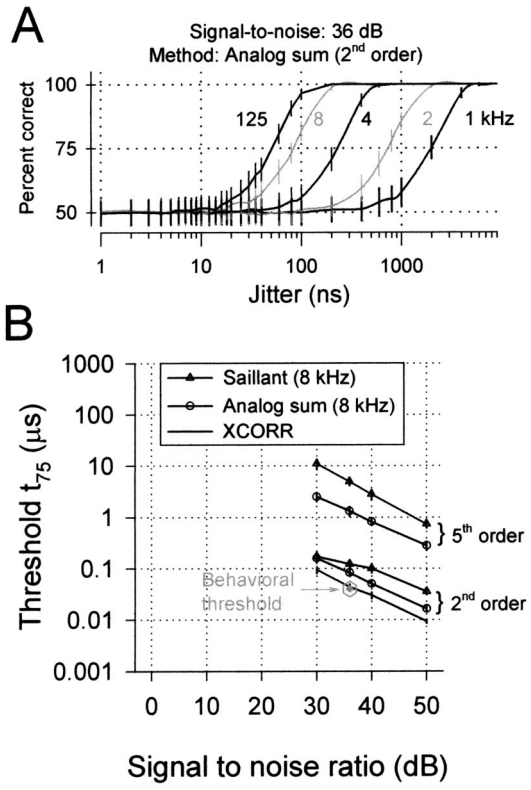

FIG. 7. Jitter threshold for single echo delay. Filterbank delay estimates from the Monte Carlo trials were used to simulate the Simmons *et al.* (1990) single echo jitter experiment (see the text). (A) The performance of the simulated bat in choosing the jittering echo at a signal-to-noise ratio of 36 dB is plotted as percent correct (± st. dev.). The low-pass filter's cutoff frequency is indicated next to each curve. Threshold was taken where the curves crossed the 75%-correct level. (B) The threshold for jitter detection for several different methods. The filterbank models used low-pass filters with an 8-kHz cutoff frequency. The behavioral threshold measured at a signal-to-noise ratio of 36 dB, from Simmons *et al.* (1990), is indicated by the gray symbol.

The simulated jitter experiment assumes the model bat uses the *minimum* number of emissions necessary for the task. In the actual behavioral experiment, the bats certainly took ''multiple looks'' at each side, using anywhere between 6 and 15 or 20 emission per side before making a decision (Simmons *et al.*, 1990). Currently, there is limited knowledge of how bats integrate information across multiple emissions. If the model bat was allowed to average delay estimates across six emissions, accuracy could improve by a factor of 2.45 (in the simulated jitter task, six emissions per side results in three jitter estimates; therefore, the model bat, assuming it had perfect memory storage of those estimates, would see an improvement of $\sqrt{3}$). Applied to the analog sum (second-order) results in Fig. 7 at 36 dB, this would improve the accuracy from 82.9 to 47.9 ns, which is similar to the observed behavioral threshold. At higher signal-to-noise ratios, use of multiple sounds led to comparable improvements in performance.

A. Implementation details for filterbank models

We did not include the effects of internal (receiver) noise upon pulse–echo delay accuracy because modeling the bat's nervous system and cognitive state requires many additional assumptions and parameters that would have to be tested. Internal noise (such as the variability in *when* or *how many* action potentials are generated by auditory neurons, or variability in the memory/decision process) has been considered elsewhere. For example, Suzuki and Suga (1991) assessed the theoretical accuracy for a topographically arranged pool of cortical neurons with variable delay-tuned responses. Their best decoder of cortical activity achieved an echo delay acuity of 800 ns. Another model used to test echo-delay accuracy, developed by Wotton *et al.* (2002), used a population of midbrain, thalamic, and cortical neurons imbued with the latency variability and delay tuning response uncertainty observed in neurophysiological experiments. Similar to Suzuki and Suga's (1991) results, this population model also had a jitter acuity of ~1 μs. Palakal and Wong (1999) also developed a model that used cortical delay-tuned neurons to estimate pulse–echo delay, but did not systematically explore its accuracy beyond reporting that the typical error was about 2%, or ~20 microseconds, of the tested target range. The distribution or variance of these errors was not reported. If possible, future models should incorporate both the effects of internal and external noise on echo delay estimation precision for comparison to the published behavioral data.

This study was motivated in part by an earlier study that documented the low accuracy of a filterbank in the echo-delay estimation task (Hackbarth, 1986). Those earlier results are worse than our filterbank with 1-kHz low-pass filtering (not shown). Several caveats must be mentioned before comparing those data to our simulation results. First, the pulse and echo signals were constructed using a recorded *Eptesicus* broadcast, which had a smaller effective signal bandwidth (it spanned 90–30 kHz) than our test signals. Second, among several differences in the earlier filterbank design, the most significant probably resides in the smoothing procedure. After bandpass filtering, Hackbarth calculated the envelope in a two-step process: she (1) computed the amplitude envelope by taking the absolute value of the signal's Hilbert transform (essentially a full-wave rectification), and (2) low-pass filtered the result at 5 kHz. No further details were provided about this low-pass filter.

The low-pass filter's effect was most deleterious for cutoff frequencies less than the *bandpass* filter bandwidth (i.e., below 4 kHz). When the low-pass filter cutoff was <4 kHz, the low-pass stage not only removes the ac component from the envelope, but more importantly begins to smear the effective integration time established by the bandwidth of the bandpass filter. For a low-pass cutoff above $\geqslant 4$ kHz, some of the ac component passes, and the effective integration time of the whole channel is unchanged, remaining at its minimum value (~250 μs, which originates in the *bandpass* filters' fixed bandwidth of 4 kHz). This surviving ac phase information is crucial for pushing echo-delay accuracy closer to the cross-correlation result (Fig. 4).

B. Low-pass filtering and inner hair cells

The results shown in Fig. 4 reveal the need to obtain constraining empirical data on the bat's inner hair cell membrane filtering properties. In order to move beyond the de-

velopment of the present peripheral auditory filterbank model we need to know both (1) the shape of the effective integration time and (2) the frequency at which ac ripple is no longer detectable in the inner hair cell membrane potential. The available data come from guinea pigs and cats (e.g., Palmer and Russell, 1986), not from bats. Recordings of the inner hair cell receptor potential evoked by pure tones typically show two components: an ac component equal in frequency to the pure tone, and a dc component. The ac component decreases in amplitude with increasing test-tone frequency, while the dc component increases reciprocally. The falloff in the ac amplitude, which for guinea pigs occurs between 0.5–2 kHz (Palmer and Russell, 1986), is due to the inner hair cell's membrane time constant (Russell and Sellick, 1978). Because acquiring data from hair cells is technically difficult, many researchers have addressed this question instead in the auditory nerve. Although the relationship between receptor potential and auditory-nerve spike triggering has not been well studied in a direct manner, for the most part it is reasonable to study phase sensitivity in the auditory nerve because, if it does not exist in the spikes traveling to the cochlear nucleus, then it cannot be detected by the auditory system. In the guinea pig, at least, the decrease in the receptor potential ac component correlates with the decrease in auditory-nerve spike phase locking (Palmer and Russell, 1986). For guinea pig and chinchilla auditory-nerve fibers, phase locking begins to fall off at 0.6 kHz and is negligible by 3.5 kHz (Harrison and Evans, 1979; Palmer and Russell, 1986). Cat auditory-nerve fibers show a gradual falloff that begins around 1–2 kHz and is near zero above 4–5 kHz (Johnson, 1980). Barn owl auditory-nerve fibers show significant phase locking up to 9 kHz (Koppl, 1997). Which of these values is appropriate for FM bats such as *Eptesicus* has yet to be determined. We are not aware of any relevant studies in bats except for one by Suga *et al.* (1971), in which two-tone ''beat'' stimuli evoked phase-locked activity up to 3 kHz in the auditory nerve of *Pteronotus parnelli*.

C. Physiological experiments

Because the neurons of interest for bats have BFs well above 10 kHz (beyond the phase-locking limit seen in birds), phase *locking* to cycles of pure tones cannot be measured. Instead of using long pure tones to measure phase *locking*, a better test for echolocating animals is one of phase *sensitivity*. For bats, important acoustic events are extremely brief FM sounds that typically evoke an average of just 1 spike per stimulus (Pollak *et al.*, 1977; Ferragamo *et al.*, 2002; Sanderson and Simmons, 2000). What matters are the relative latencies of these single spikes across neurons, each of which is evoked by a pulse or echo after a relatively brief period of quiet. Do neurons show latency shifts when the phase of a brief tone burst or FM sweep changes?

Thus far, we have conducted a series of experiments in the brainstem and inferior colliculus of *Eptesicus fuscus* to test this question. Local field potentials do show sensitivity (changes in shape) to changes in pure-tone burst starting phase (Ferragamo *et al.*, 2002). This sensitivity to phase can be observed for pure tones up to 16 kHz. Results from these physiological experiments address findings from experiments in *Eptesicus* that imply (behavioral: Menne *et al.*, 1989; Simmons *et al.*, 1990; Moss and Simmons, 1993) or require (computational: Peremans and Hallam, 1998; Matsuo *et al.*, 2001; Neretti *et al.*, 2003; Saillant *et al.*, 1993) phase sensitivity in the ultrasonic range.

ACKNOWLEDGMENTS

Grants from NSF (BES-9622297) and ONR (N00014-99-1-0350) to J.A.S., an NIH Training grant, and a Burroughs-Wellcome grant to the Brown University Brain Sciences Program supported this work.

Altes, R. A. (**1984**). ''Echolocation as seen from the viewpoint of radar/sonar theory,'' in *Localization and Orientation in Biology and Engineering*, edited by D. Varju and H.-U. Schnitzler (Springer, Berlin), pp. 234–244.

Beedholm, K., and Mohl, B. (**1998**). ''Bat sonar: An alternative interpretation of the 10-ns jitter result,'' J. Comp. Physiol., A **182**, 259–266.

Burdic, W. S. (**1968**). *Radar Signal Analysis* (Prentice-Hall, New York).

Cariani, P. A., and Delgutte, B. (**1996**). ''Neural correlates of the pitch of complex tones. I. Pitch and pitch salience,'' J. Neurophysiol. **76**, 1698–1716.

Dear, S. P., Simmons, J. A., and Fritz, J. (**1993**). ''A possible neuronal basis for representation of acoustic scenes in auditory cortex of the big brown bat,'' Nature (London) **364**, 620–623.

Feng, A. S., Simmons, J. A., and Kick, S. A. (**1978**). ''Echo detection and target ranging neurons in the auditory system of the bat *Eptesicus fuscus*,'' Science **202**, 645–648.

Ferragamo, M. J., Sanderson, M. I., and Simmons, J. A. (**2002**). ''Phase sensitivity of auditory brain-stem responses in echolocating big brown bats,'' J. Acoust. Soc. Am. Suppl. **112**, S-2288.

Grinnell, A. D. (**1995**). ''Hearing in bats: an overview ,'' in *Hearing by Bats*, edited by A. N. Popper and R. R. Fay (Springer-Verlag, New York), pp. 1–36.

Hackbarth, H. (**1986**). ''Phase evaluation in hypothetical receivers simulating ranging in bats,'' Biol. Cybern. **54**, 281–287.

Harrison, R. V., and Evans, E. F. (**1979**). ''Some aspects of temporal coding by single cochlear fibers from regions of cochlear hair cell degeneration in the guinea pig,'' Arch. Oto-Rhino-Laryngol. **224**, 71–78.

Johnson, D. J. (**1980**). ''The relationship between spike rate and synchrony in responses of auditory nerves to single tones,'' J. Acoust. Soc. Am. **68**, 1115–1122.

Koay, G., Heffner, H. E., and Heffner, R. S. (**1997**). ''Audiogram of the big brown bat (*Eptesicus fuscus*),'' Hear. Res. **105**, 202–210.

Koppl, C. (**1997**). ''Phase locking to high frequencies in the auditory nerve and cochlear nucleus magnocellularis of the barn owl, *Tyto alba*,'' J. Neurosci. **17**, 3312–3321.

Matsuo, I., Tani, J., and Yano, M. (**2001**). ''A model of echolocation of multiple targets in 3D space from a single emission,'' J. Acoust. Soc. Am. **110**, 607–624.

Menne, D. (**1988**). ''A matched filter bank for time delay estimation in bats,'' in *Animal sonar: Processes and Performance*, edited by P. E. Nachtigall and P. W. B. Moore (Plenum Press, New York), pp. 835–842.

Menne, D., Kaipf, I., Wagner, I., Ostwald, J., and Schnitzler, H. U. (**1989**). ''Range estimation by echolocation in the bat *Eptesicus fuscus*: Trading of phase versus time cues,'' J. Acoust. Soc. Am. **85**, 2642–2650.

Menne, D., and Hackbarth, H. (**1986**). ''Accuracy of distance measurement in the bat *Eptesicus fuscus*: Theoretical aspects and computer simulations,'' J. Acoust. Soc. Am. **79**, 386–397.

Moss, C. F., and Schnitzler, H.-U. (**1989**). ''Accuracy of target ranging in echolocating bats: Acoustic information processing,'' J. Comp. Physiol. A **165**, 383–393.

Moss, C. F., and Schnitzler, H.-U. (**1995**). ''Behavioral studies of auditory information processing,'' in *Hearing by Bats*, edited by A. N. Popper and R. R. Fay (Springer-Verlag, New York), pp. 87–145.

Moss, C. F., and Simmons, J. A. (**1993**). ''Acoustic image representation of a point target in the bat *Eptesicus fuscus*: Evidence for sensitivity to echo phase in bat sonar,'' J. Acoust. Soc. Am. **93**, 1553–1562.

Neretti, N., Sanderson, M. I., Intrator, N., and Simmons, J. A. (**2003**). ''Time-frequency computational model for echo-delay resolution in sonar images of the big brown bat, *Eptesicus fuscus*,'' J. Acoust. Soc. Am. **113**, 2137–2145.
O'Neill, W. E. (**1995**). ''The bat auditory cortex,'' in *Hearing by Bats*, edited by A. N. Popper and R. R. Fay (Springer-Verlag, New York), pp. 416–480.
O'Neill, W. E., and Suga, N. (**1982**). ''Encoding of target range and its representation in the auditory cortex of the mustached bat,'' J. Neurosci. **2**, 17–31.
Palmer, A. R., and Russell, I. J. (**1986**). ''Phase-locking in the cochlear nerve of the guinea-pig and its relation to the receptor potential of inner hair cells,'' Hear. Res. **24**, 1–15.
Palakal, M. J., and Wong, D. (**1999**). ''Cortical representation of spatiotemporal pattern of firing evoked by echolocation signals: Population encoding of target features in real time,'' J. Acoust. Soc. Am. **106**, 479–490.
Peremans, H., and Hallam, J. (**1998**). ''The spectrogram correlation and transformation receiver revisited,'' J. Acoust. Soc. Am. **104**, 1101–1110.
Pollak, G. D., Marsh, D. S., Bodenhamer, R., and Souther, A. (**1977**). ''Characteristics of phasic-on neurons in the inferior colliculus of anaesthetized bats with observations related to mechanisms for echoranging,'' J. Neurophysiol. **40**, 926–941.
Pollak, G. D. (**1993**). ''Some comments on the proposed perception of phase and nanosecond time disparities by echolocating bats,'' J. Comp. Physiol. A **172**, 523–531.
Russell, I. J., and Sellick, P. M. (**1978**). ''Intracellular studies of hair cells in the mammalian cochlea,'' J. Physiol. (London) **284**, 261–290.
Saillant, P. A., Simmons, J. A., Dear, S. P., and McMullen, T. A. (**1993**). ''A computational model of echo processing and acoustic imaging in frequency-modulated echolocating bats: The spectrogram correlation and transformation receiver,'' J. Acoust. Soc. Am. **94**, 2691–2712.
Sanderson, M. I., and Simmons, J. A. (**2000**). ''Neural responses to overlapping FM sounds in the inferior colliculus of echolocating bats,'' J. Neurophysiol. **83**, 1840–1855.
Schnitzler, H. U., and Henson, O. W. (**1980**). ''Performance of airborne animal sonar systems: Michrochiroptera,'' in *Animal Sonar Systems*, edited by P. E. Nachtigall and P. W. B. Moore (Plenum, New York), pp. 109–181.
Schnitzler, H.-U., Menne, D., and Hackbarth, H. (**1985**). ''Range determination by measuring time delays in echolocating bats,'' *Time Resolution in Auditory Systems*, edited by A. Michelsen (Springer, Berlin), pp. 180–204.
Simmons, J. A. (**1973**). ''Resolution of target range by echolocating bats,'' J. Acoust. Soc. Am. **54**, 157–173.
Simmons, J. A. (**1980**). ''The processing of sonar echoes by bats,'' in *Animal Sonar Systems*, edited by R.-G. Busnel and J. F. Fish (Plenum, New York), pp. 695–714.
Simmons, J. A. (**1993**). ''Evidence for perception of fine echo delay and phase by the FM bat, *Eptesicus fuscus*,'' J. Comp. Physiol., A **172**, 533–547.
Simmons, J. A., Ferragamo, M., Moss, C. F., Stevenson, S. B., and Altes, R. A. (**1990**). ''Discrimination of jittered sonar echoes by the echolocating bat, *Eptesicus fuscus*: The shape of target images in echolocation,'' J. Comp. Physiol., A **167**, 589–616.
Simmons, J. A., and Grinnell, A. D. (**1988**). ''The performance of echolocation: Acousitc images perceived by echolocating bats,'' in *Animal Sonar: Processes and Performance*, edited by P. Nachtigall and P. W. B. Moore (Plenum, New York), pp. 353–385.
Suga, N. (**1971**). ''Responses of inferior collicular neurones of bats to tone bursts with different rise times,'' J. Physiol. (London) **217**, 159–177.
Sullivan, W. E. (**1982**). ''Neural representation of target distance in auditory cortex of the echolocating bat *Myotis lucifugus*,'' J. Neurophysiol. **48**, 1011–1032.
Suzuki, M., and Suga, N. (**1991**). ''Acuity in ranging based upon neural responses in the FM–FM area of the mustached bat,'' Program No. 181.8, Soc. Neuroscience Abstract.
Weiss, T. F., and Rose, C. (**1988**). ''A comparison of synchronization filters in different auditory receptor organs,'' Hear. Res. **33**, 175–188.
Wotton, J., Sanderson, M. I., and Ferragamo, M. J. (**2002**). ''Simulating temporal 'jitter' discriminations using three populations layers of bat auditory neurons,'' Program No. 762.8, Soc. Neuroscience Abstract.